STUDY OF THERMAL CONDUCTIVITY IN BULK CRYSTAL AND KAPITZA CONDUCTANCE AT GRAIN BOUNDARIES OF STRONTIUM TITANATE BY MOLECULAR DYNAMICS SIMULATION

By

ZEXI ZHENG

A THESIS PRESENTED TO THE GRADUATE SCHOOL
OF THE UNIVERSITY OF FLORIDA IN PARTIAL FULFILLMENT
OF THE REQUIREMENTS FOR THE DEGREE OF
MASTER OF SCIENCE

UNIVERSITY OF FLORIDA

2013

To my father and mother, for their support

ACKNOWLEDGMENTS

I would like to express sincere gratitude to my advisor Dr. Youping Chen first, for her support and encouragement. Then, I'd like to thank my committee member: Dr. Curtis Taylor, for the willingness to review my work. Special thanks are given to Dr. Liming Xiong, for his advice and valuable comments. Also, I want to express my appreciation to my fellows in the lab: Xiang Chen, Shengfeng Yang, Ning Zhang, Shikai Wang, Chen Zhang, and Rui Che.

TABLE OF CONTENTS

page

LIST OF TABLES

LIST OF FIGURES

LIST OF ABBREVIATIONS

AMM	Acoustic mismatch model
CSL	Coincidence site lattice
DMM	Diffuse mismatch model
GB	Grain boundary
MD	Molecular dynamics
TE	Thermoelectric

Abstract of Thesis Presented to the Graduate School
of the University of Florida in Partial Fulfillment of the
Requirements for the Degree of Master of Science

STUDY OF THERMAL CONDUCTIVITY IN BULK CRYSTAL AND KAPITZA CONDUCTANCE AT GRAIN BOUNDARIES OF STRONTIUM TITANATE BY MOLECULAR DYNAMICS SIMULATION

By

Zexi Zheng

May 2013

Chair: Youping Chen
Major: Mechanical Engineering

Perovskite-type $SrTiO_3$ as a potential thermoelectric material has attracted great attention. Although it shows a high factor in the figure of merit, the high thermal conductivity value is still not satisfactory. Nanostructuring approaches reveal the ability to modify the overall thermal transport performance; but before that, we need to know which type of grain boundary and what kind of structure has the highest thermal resistance. Therefore, studies on thermal properties at $SrTiO_3$ GBs will have great significance.

We first measure the thermal conductivity of $SrTiO_3$ bulk crystal using the nonequilibrium molecular dynamics simulation and systematically explore the related issues coming with the method. The results are extrapolated and compared with those from experiments and other simulations, which shows a reasonable agreement, indicating that the method works well with the material studied here. Then, four bicrystal systems with different symmetric tilt grain boundaries (Σ 5(310), Σ 5(210), Σ 13(510) stable, and Σ 13(510) metastable) are modeled and their Kapitza conductance at grain boundaries are evaluated by simulations using the same, well tested technique. We

compare the results and find the Kapitza conductance depends on the amount of disorder at grain boundary region most, but doesn't show direct relationship with the GB energy. We also find the voids and gaps may impede the thermal transport and their density along the grain boundary plays an important role. Finally, we notice that temperature discontinuities measured at the two grain boundaries are slightly different in each case. The two GBs have exactly the same structure but face towards opposite directions. That means the side from which the incident heat current comes also matters, which suggests that the pattern of an incident plane may be a factor to influence the thermal transport. However, further investigations on larger systems and studies about phonon wave dynamics will be necessary in order to elucidate this.

CHAPTER 1
INTRODUCTION

Thermoelectric (TE) materials have attracted great attention since they can interconvert a temperature difference and an electric potential directly and be applied to a variety of areas. The perovskite-type $SrTiO_3$ has been recognized as a prospective good n-type thermoelectric material, since it shows a high power factor of $2.3\times10^{-3}\ Wm^{-1}K^{-2}$ [1] for $S^2\sigma$ in the dimensionless figure of merit $ZT = S^2\sigma T/\kappa$, where S is the Seebeck coefficient, σ the electrical conductivity, κ the thermal conductivity and T the absolute temperature. However, the ZT value is still too low for practical applications due to the relative high intrinsic thermal conductivity value of about $11\ Wm^{-1}K^{-1}$ at room temperature.[2] Recent studies have found that nano-grained structures show much lower thermal conductance since enhanced phonon scattering occurs at grain boundaries,[3,23] which will greatly reduce the κ value. Thus, nanostructuring approaches reveal the large potential to modify the overall thermal transport performance without deteriorating $S^2\sigma$. But before that, we need to know which type of grain boundary and what kind of structure has the highest thermal resistance. Therefore, studies on thermal properties at $SrTiO_3$ grain boundaries will have great significance.

The objective of this work is to measure and compare the Kapitza conductance at $SrTiO_3$ tilt grain boundaries. A proper simulation method is first chosen and evaluated through the measurement of thermal conductivity values of $SrTiO_3$ bulk crystals. Then the well tested and defined techniques are applied to study the Kapitza conductance at four $SrTiO_3$ tilt grain boundaries. The following work is organized as follows: In Chapter 2, background and related works are introduced; In Chapter 3, measurement of thermal

conductivity of bulk crystal systems will be carried out and related issues with the method will be systematically explored and discussed; Chapter 4, which is the main part, will employ the techniques evaluated and further determined in Chapter 3 to perform simulations on $SrTiO_3$ bicrystal systems and compare the Kapitza conductance resulting at different tilt grain boundaries.

CHAPTER 2
BACKGROUND AND RELATED WORK

Strontium Titanate

Strontium titanate ($SrTiO_3$) or STO is a perovskite-type oxide of strontium and titanium, one of the most common ceramics. It has a crystallographic cubic structure with the space group number 221 and a lattice constant of 3.9049 angstroms, which is similar to a diamond. The 5-atom unit cell structure is shown in Figure 2-1.

Recent studies on strontium titanate have shown its great potential for practical applications, such as: the usage in fuel cells, steam electrolysis and hydrogen gas sensors[4-6] because of its high photonic conductivity at high temperature; the usage as substrates for the fabrication of high-Tc superconducting films and devices for its favorable dielectric constant 277 and the good lattice match; and employment in power generation through recovered waste heat or electronic refrigeration for electronic devices[7] due to its good thermoelectric properties.

Since substantial achievements have been made on using thermoelectric materials to interconvert the temperature gradient and the electrical potential, the promising technology attracts much attention recently. STO presents a high power factor $S^2\sigma$ in figure of merit ZT, which indicates it's a good potential TE material. But its thermal conductivity value is still relatively too high; more efforts will be needed before it can be put into practical applications. Therefore, researchers made some attempts to try to reduce the κ value: Wang and his co-workers[3] examined a series of nanograined dense $SrTiO_3$ ceramics and found the κ decreased with decreasing the average grain size, which is mainly due to the increase of interfaces as heat barriers. Chernatynskiy and his co-workers[8] analyzed the thermal transport properties of the Ruddlesden-

Popper phase, formed by interleaving perovskite layers of $SrTiO_3$ with strontium oxide rocksalt layers and found a difference between the thermal properties measured parallel to the structural layering and those measured perpendicular to the layering. Muta and his co-workers,[9] by contrast, studied the reduced and La-doped single-crystalline $SrTiO_3$. Their results show that both electrical conductivity and thermal conductivity are lower in reduced sample and oxygen vacancies will cause strong electron and phonon scattering.

Brief Introduction to Molecular Dynamics Simulation

The molecular dynamics method (MD) was first introduced by Alder and Wainwright in the late 1950's. The purpose of the method was to study the interactions of hard spheres. But later, insights concerning behaviors of simple liquids were developed. Since MD simulations deal with and generate information only at the atomistic level, knowledge on statistical mechanics is required to convert information from microscopic level to macroscopic level or vice versa.

The MD simulation method is based on Newton's second law or the equation of motion, $F = ma$, which means it's purely classical. This may result in some problems, because systems at the atomistic level obey quantum laws rather than classical laws. Furthermore, quantum effects become critically important when system temperature is below the Debye temperature. To avoid such issues, our models are generated as large as possible and simulated over the Debye temperature, i.e. 600K, for $SrTiO_3$.

Remarkably, various interaction types are supported in MD, but we have to provide our own parameters. The potential function we use here is a combination of Buckingham and Coulombic force, which has a relative low computational efficiency, since a long cut-off distance will include a vast number of atoms, resulting in a long computing time. We will employ the parameters fit by Thomas et al.[10]

Several Methods for Phonon-Mediated Thermal Transport Investigations by Simulation

We have several different simulation-based approaches that can be used to study the thermal conductance of a material. Among them, the most remarkable one should be phonon wave-packet dynamics, which was developed to provide a way to gain detailed insight into the mechanism of phonon scattering at interfaces. The method first creates phonon wave packets that are superposition of normal modes at one end of a specimen, then lets the wave packets propagate towards another end using molecular dynamics simulation. After they reach the interface, some of them will pass through and some will be reflected back. The energy transmission coefficient can thus be determined for every polarization and wave vector. Although it's a powerful and comprehensive way to learn detailed information on how different phonon waves interact with different interface configurations, it doesn't seem to be easy when dealing with complex systems, such like the cases considered here.

The Green-Kubo method, a representation of equilibrium MD approach, can be employed to measure the thermal conductivity of a homogeneous system, as mentioned previously. Nevertheless, it is not appropriate to apply it into an inhomogeneous system especially when there involves localized features such as GBs studied here, for the Green-Kubo formalism was designed to handle situations being homogeneous only.

Another approach, the nonequilibrium MD simulation method, which has already been successfully employed to calculate the thermal conductivity in the bulk crystal Si systems, will also be introduced here. Since it's a method analogous to experiments, it is much more generous. As a result, it is capable of dealing with both homogeneous and inhomogeneous situations. Although the direct method has some limitation in the

ability of extracting detailed information regarding the phonon waves contacting with boundaries, it has another big advantage: being able to determine the Kapitza conductance σ_k within a single simulation.

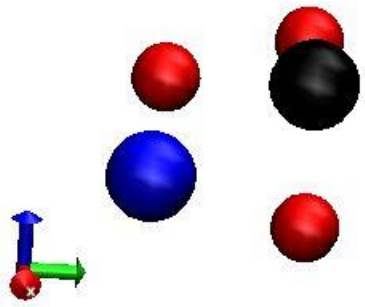

Figure 2-1. Structure of the 5-atom unit cell of $SrTiO_3$. Blue: Strontium; Black: Titanium; Red: Oxygen.

CHAPTER 3
MEASUREMENT OF THERMAL CONDUCTIVITY OF STRONTIUM TITANATE BULK CRYSTAL

We have already known that there are two common techniques for computing thermal conductivity by atomic-level simulation, direct method and Green-Kubo method. Since the Green-Kubo method requires the simulation process to be very long in order to achieve convergence, it's not suitable to be employed here for the ionic-bonded material simulation, which is quite expensive in computational resource. Thus, the direct method will be chosen to perform our simulations. In this chapter, we will systematically explore the issues related to the measurement of thermal conductivity when using direct method. For the purpose of getting a relative good result that comparable to those from experiments, the simulation time necessary for the system to achieve dynamic equilibrium, the heat current loaded, and the temperature dependence, these aspects will be examined. And lastly, the system size effect, which has a significant influence on the on the measured thermal conductivity value will be considered.

Modeling of Strontium Titanate Bulk Crystal

The crystal structure of the perovskite type $SrTiO_3$ is cubic. This greatly simplifies the modeling procedure of a single crystal. As we can see from Figure 3-2, the final three-dimensional rectangular model can be obtained by extending the cubic unit cell in three perpendicular directions, namely, the x, y and z directions. As an example here, if we want to generate a model with its dimension 4 by 4 by 51 unit cells, simply duplicate the 5-atom unit cell 4 times along x and y direction and 51 times along z direction. Make sure the two adjacent cells are end to end and to keep a lattice constant distance between them. After the model is finished, the spatial coordinates of each atom along

with their atom type and charge value must be printed into a data file that can be recognized by Lammps as an input file.

Molecular Dynamics Simulation of Thermal Conductivity Measurement for the Single Crystal System

In this section we demonstrate how the thermal conductivity value for a single crystal system is measured by direct method. Figure 3-1 shows the three-dimensional periodic simulation cell for measuring the bulk crystal thermal conductivity. It has the exact same size as that of the simulation model we created since periodic boundary conditions will be applied to all six borders in order to make the results as accurate as possible. At each side of the cell, there's a region in the middle, where atom velocities are rescaled in every MD step. As we can see in the figure, some amount of energy $\Delta\varepsilon$ is added into the region on the left by rescaling the particle velocities; meanwhile, the same amount of energy is subtracted from the region on the right. This will result in a thermal current flowing from the hot end (heat source) to the cool end (heat sink), as indicated in the figure. Due to the periodicity of the left and right two boundaries, the energy flow will split into two same parts, one going towards right and the other going towards left. The part to the left will leave the left border first and then come back from right border again, finally reach the heat sink.

The whole procedure is made up of four major steps: initiating velocity, environmental temperature control (0 ~ 40,000 MD step), microcanonical relaxation (40,000 ~ 70,000 MD step) and applying the heat flux (70,000 ~ 2,000,000 MD step). The first step is to give an ensemble of velocities based on the aimed temperature designated to all the particles of the system. Since the initial temperature measured according to the initial velocities will drop to about a half in the following steps, we may

set it to be twice higher. As it can be seen from Figure 3-3A, the initial temperature was firstly set to be 900 K, then it went down to about 600 K. The second step is to apply the canonical ensemble control (NVT) to adjust and maintain the system mean temperature at the desired ambient temperature. As we can see from Figure 3-3B, the average temperature of the whole system is kept around 600K. However, the NVT algorithm can't be that precise to adjust the temperature to exact 600K, which is also not necessary. Figure 3-4 shows the necessity of applying the third step, microcanonical ensemble control (NVE), also known as relaxation. From the diagram, we see the temperature distribution along z direction is quite uneven although the mean temperature is 600 K, if only NVT control is applied. But after 30,000 steps of relaxation, it's much smoother; what's more, the temperature peak originally in the middle is vanished. Lastly, a steady heat flux is applied to the system by rescaling the particle velocities at the two slabs.

The final temperature profile is shown in Figure 3-5, which is obtained by averaging all data gathered through step 500,000 to step 2,000,000. It is found that the system may be able to reach a steady state after 200,000 steps of heat flux is applied and a span of 1,500,000 steps should be long enough to produce a smooth and nice temperature profile for gradient measurement. Figure 3-6 shows how we measure the temperature gradient from the temperature distribution curve. We simply make a linear fit for the two regions far away from the heat source and the heat sink, who display the strong nonlinearity of temperature distribution. For the region in the middle, it's fairly straightforward, just set the interval, and do the linear fit; but for the region made up with the two parts adjacent to the simulation box, we need to cut them out first, and then

make a perfect match, since there are periodic boundary conditions at the simulation box borders. After they are spliced together, a linear fit can then be made.

Results and Discussion

The temperature gradient values measured for the two linear regions of the $4\times4\times51$ system, at the mean temperature of 600K, are 1.3543 K/Å and 1.3732 K/Å respectively. Then take the average, and apply Fourier's law:

$$\kappa = -\frac{q}{\Delta T}, \tag{3-1}$$

we get the thermal conductivity of the system to be: 6.5664 W/mK. For here, the heat flux q applied is: $1.791\times10^{11}\ W/m^2$.

It's not difficult to measure the thermal conductivity value for a given system, but it seems not easy to answer how valid and how good the result is; some issues related closely to the direct method need to be further examined. Also, the finite size effect must be taken into consideration.

Effect of Heat Current Density Applied

The issue is also known as the effect of deviation from Fourier's law. This may occur when the heat current applied is too large, that the system shows nonlinear response. Figure 3-8 shows the effect of changing the heat current applied to the system. The diagram is plotted as thermal conductivity value versus heat current intensity, which should be a horizontal straight line if there's no deviation from Fourier's law, i.e. the κ value remains constant. However, we find thermal conductivity goes up with increase of heat flux, especially when the applied heat flux exceeds $3*\Delta\varepsilon$, where $\Delta\varepsilon = 5\times10^{-4}$ ev (corresponding to q=0.597e11 W/m^2). Thus, to comply with Fourier's law, we may use any value between $2*\Delta\varepsilon$ and $3*\Delta\varepsilon$, since in this range, least

deviation is observed. And due to the low efficiency of the computational process, it's necessary to apply the stimulation as strong as possible to save response time. We will thereby choose the value of $3*\Delta\varepsilon$ for the remaining studies.

Dependence of Thermal Conductivity on Cross-Sectional Area

Although periodic boundary conditions are applied along x and y directions and heat current travels only along z direction, there is still some size effect that will affect our results. As we have already known from the relationship:

$$\kappa = \frac{1}{\Omega} k_B v l \sum_{k_x k_y k_z} \frac{k_z^2}{k^2}, \tag{3-2}$$

that the summation can be different for systems with small or irregular cross sections, we must establish the bottom line below which the values measured are invalid. The results are shown in Figure 3-9 and 3-10, where the former reveals the influence of cross-sectional size on κ values and the latter shows how the temperature profile of each case looks like. We see the thermal conductivity values measured for the systems of size 3*3 and 4*4 match well while those measured for systems with sizes 1*1 and 2*2 deviate a lot. This can be understood by inspecting the four temperature profiles. The temperature distribution curves of the two cases, 1*1 and 2*2, are not even stable, which may be caused by the insufficient number of atoms in a slice that statistical averaging is based on. The results suggest that in order to get a smooth and nice temperature profile for the further measurement of thermal conductivity, a system with the cross section size at least 3 by 3 unit cells will be needed.

Dependence of Thermal Conductivity on Temperature

Figure 3-11 shows the dependence of thermal conductivity on environmental temperatures for the system of size 4*4*51 unit cells. We see the κ value decreases

with increasing the ambient temperature, which is a typical property for phonon-mediated thermal transport. The values and trend can be compared with those results from experiments (Figure 3-7A, by Yamanaka et al.) and simulations (Seetawan et al.), and they are in good agreement.

Finite Size Effect

Finally, the finite size effect must be taken into account since it's quite important. Finite size effects arise when the length of the simulation cell (Lz) is not significantly longer than the phonon mean-free path. Strictly speaking, the results we got above cannot be compared to those from experiments since specimens used for investigations in real life are far much longer. But the good news is, the effect can be reliably eliminated by doing multiple simulations of different size systems and making an extrapolation of the results to an infinite size.

The results are shown in Table 3-1 and Figure 3-12. The thermal conductivity extrapolated for the infinite-sized system at the ambient temperature of 600K is 9.9119 W/mK, which is larger than the results from experiments, but in good agreement with those reported by Chernatynskiy et al.[11]

Table 3-1. Thermal conductivity values measured from systems with different sizes at T=600K.

Lz(nm)	1/Lz(1/nm)	κ (W/mK)	$1/\kappa$ (mK/W)
40	0.025	8.1569	0.1226
28.5065	0.03508	8.06	0.1241
16.7915	0.05955	6.4129	0.1559
14.4485	0.06921	6.1228	0.1633
10.1527	0.0985	5.4429	0.1837

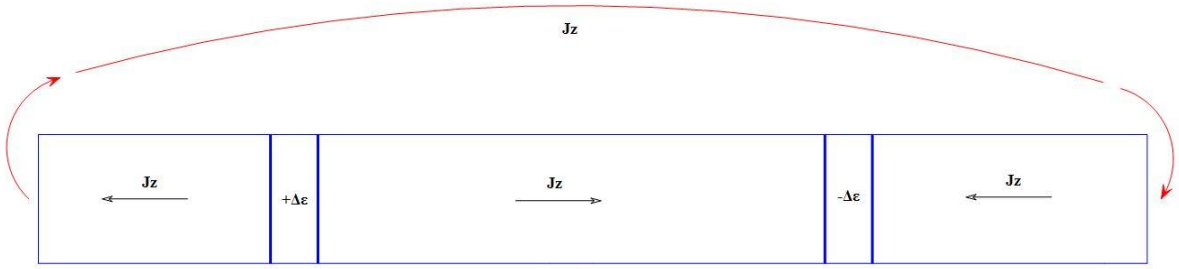

Figure 3-1. Three-dimensional periodic simulation cell for measuring the bulk crystal thermal conductivity.

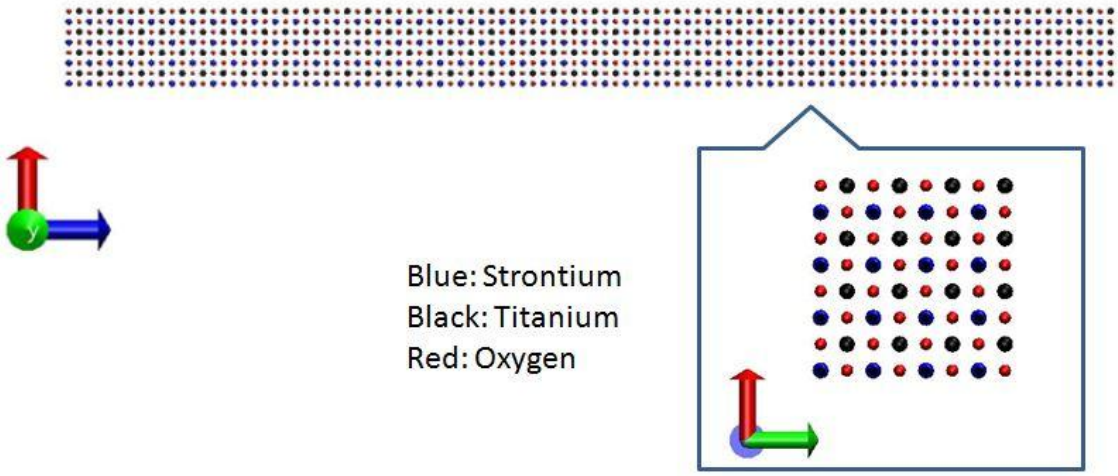

Figure 3-2. Three-dimensional bulk crystal simulation model, with a total of 4080 atoms. The size of the model is $4\times4\times51$ unit cells.

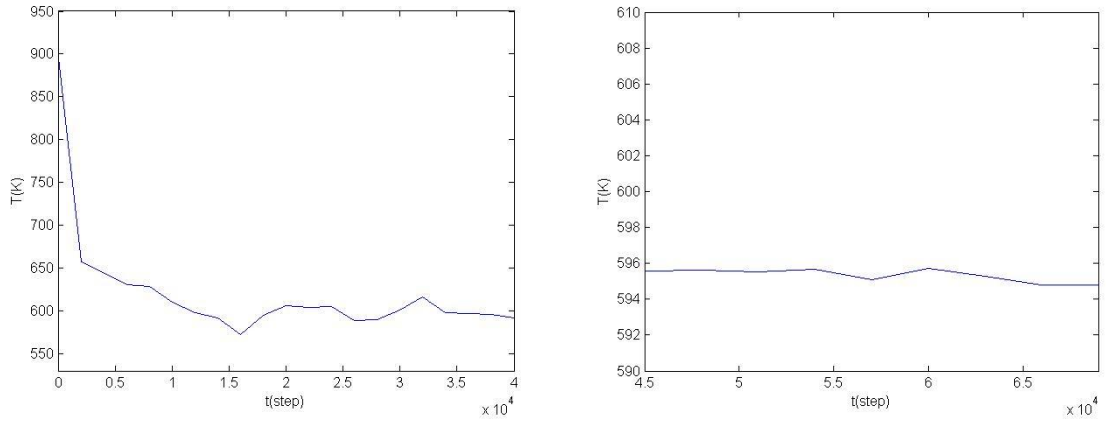

A B

Figure 3-3. Evolution of the mean temperature of the whole system from 0 ~ 70,000 time step. A) 0 ~ 40,000 time step, B) 45,000 ~ 70,000 time step.

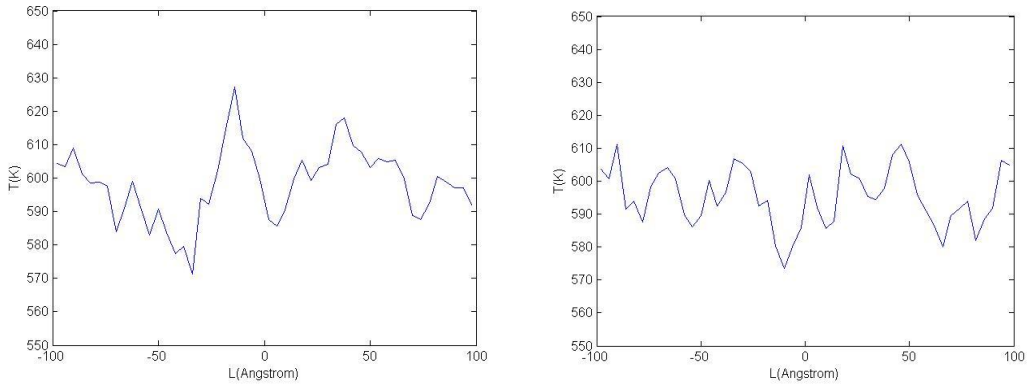

A B

Figure 3-4. Time averaged temperature distribution along z direction. A) averaged through 0 ~40,000 time step, B) averaged through 40,000 ~70,000 time step.

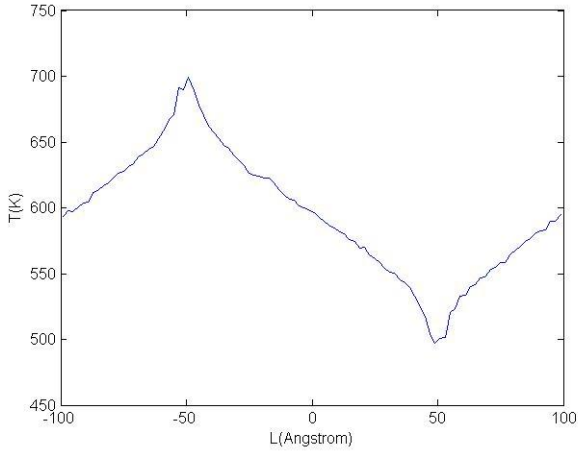

Figure 3-5. Final temperature profile of the whole system along z direction, time averaged from 500,000 to 20,00,000 MD step.

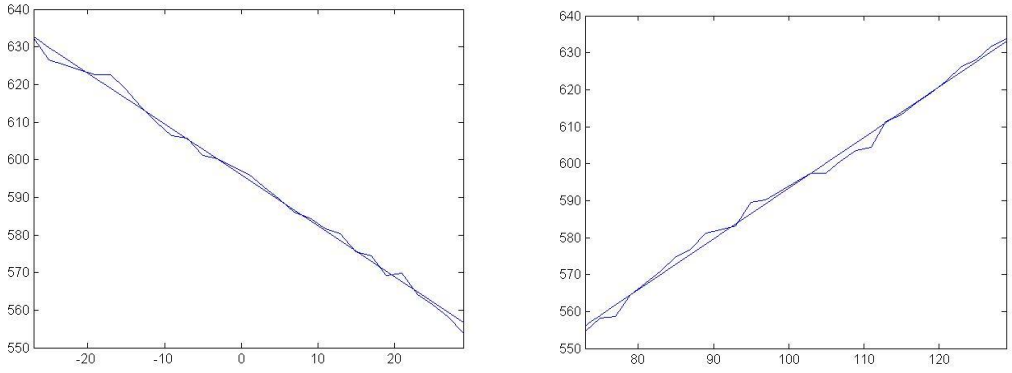

A B

Figure 3-6. Temperature profile linear fitting. A) region from -30 Å to 30 Å, B) region from 70 Å to -70 Å. (The two regions; 70 ~ right boundary and left boundary ~ -70 are joined together due to the periodicity of the boundary conditions.)

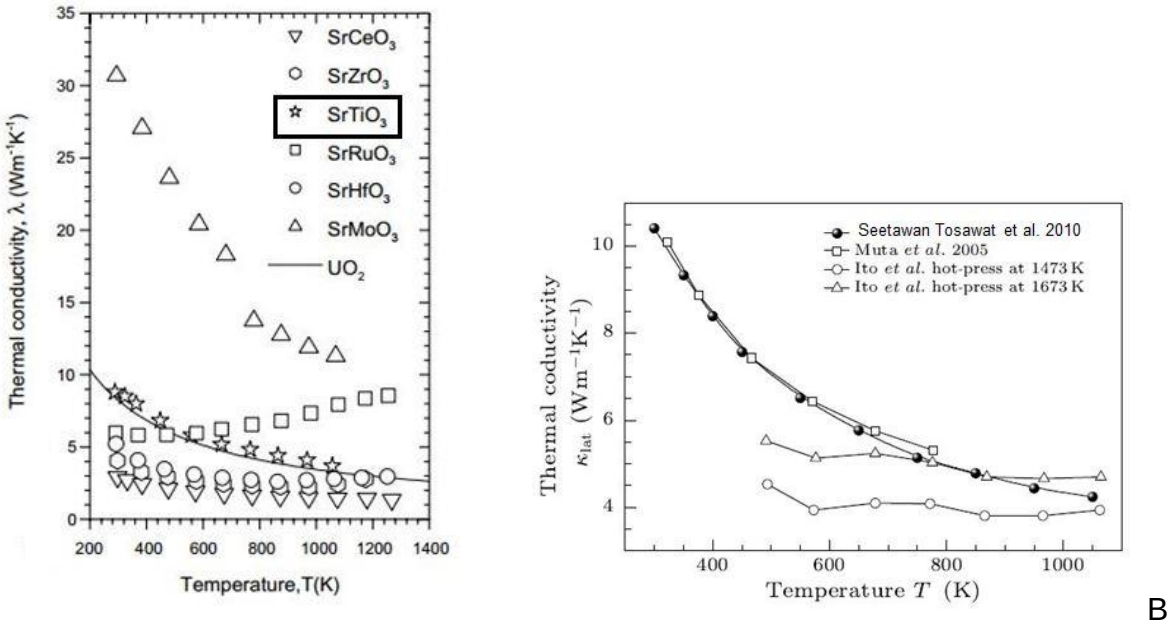

A B

Figure 3-7. Results of thermal conductivity values of $SrTiO_3$ by others. A) from Yamanaka et al.[12] by experiment, B) from Seetawan et al.[13] by MD simulation.

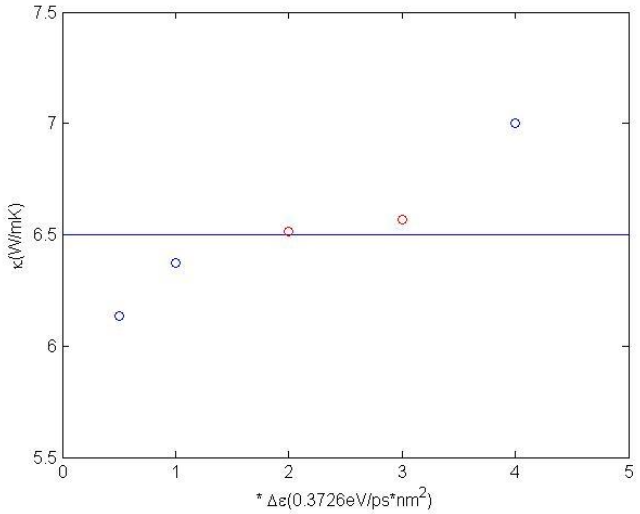

Figure 3-8. Effect of changing heat current applied to the simulation system, at an average temperature of 600K.

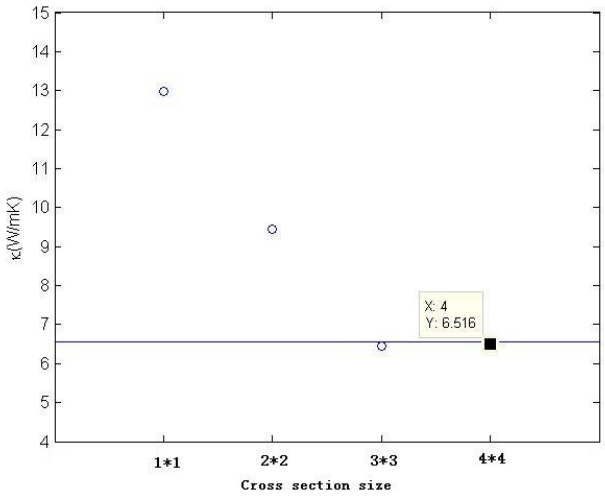

Figure 3-9. Comparison of thermal conductivity values measured under systems with different cross section sizes.

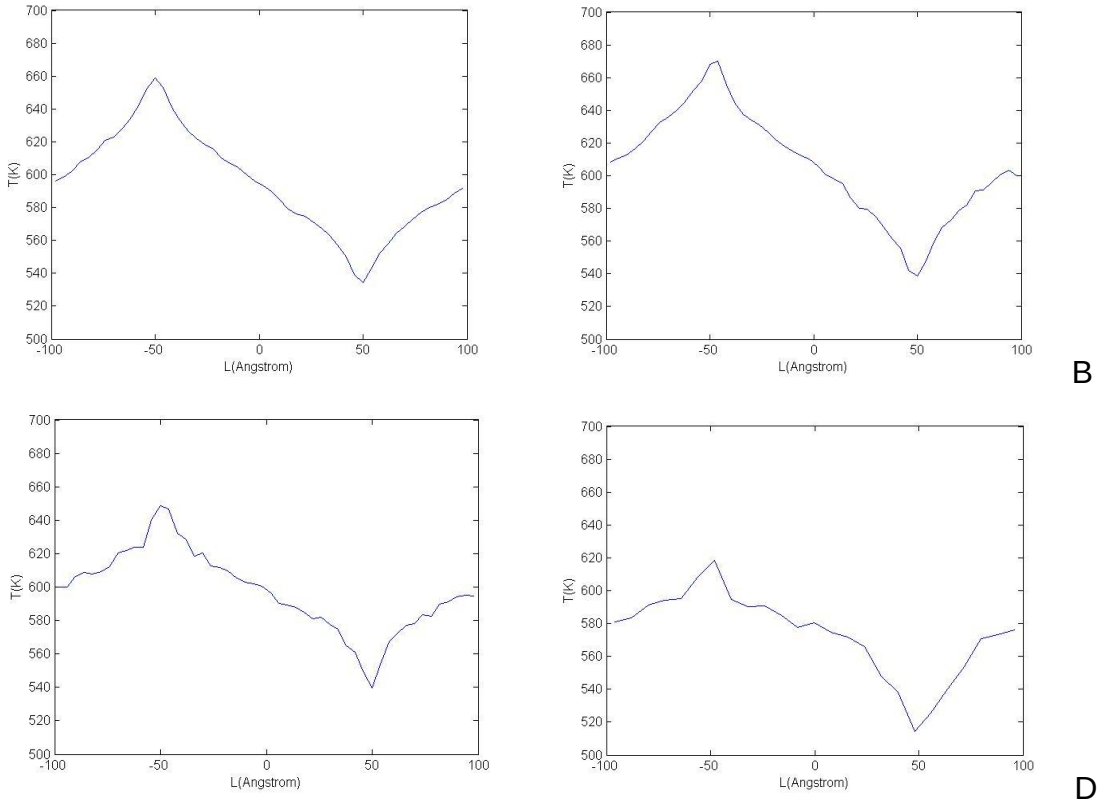

A B C D

Figure 3-10. Temperature profiles for systems with different cross section sizes. Each case was averaged through step 500,000 to step 2,000,000. A) 4 by 4 unit cells, B) 3 by 3 unit cells, C) 2 by 2 unit cells, D) 1 by 1 unit cells.

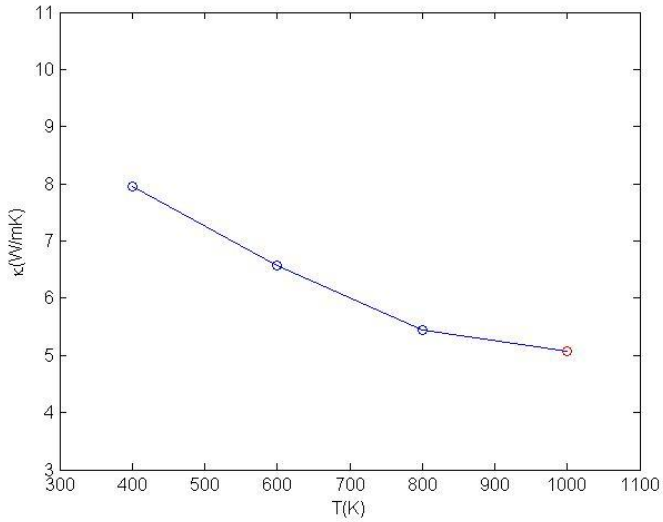

Figure 3-11. The dependence of thermal conductivity on environmental temperatures for the system of the size 4*4*51 unit cells.

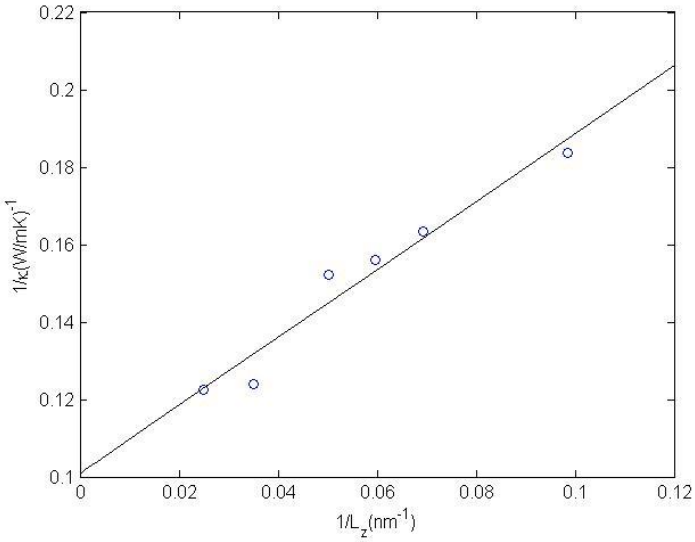

Figure 3-12. The dependence of thermal conductivity values on system sizes, under the ambient temperature of 600K. A linear fit is made to determine the thermal conductivity obtained by taking the reciprocal of the $1/\kappa$ value at $1/L_z = 0$ of the infinite system.

CHAPTER 4
STUDY OF KAPITZA CONDUCTANCE OF TILT GRAIN BOUNDARIES IN STRONTIUM TITANATE

Overview

It's known that semiconducting $SrTiO_3$ polycrystals are broadly used as varistors, for they show good nonlinear current-voltage (I-V) characteristics.[14,15] This suggests that investigations on defects and grain boundaries (GB) are indispensable. Also, some application of $SrTiO_3$ crystals (STO) such as the use of bicrystalline STO substrates as templates for Josephson junctions fabrication demands the understanding of GB structure,[16-18] which further confirms the importance of grain boundaries and defects studying.

Among the numerous properties of this ionically bonded material, those related with thermal transport have attracted significant interest as mentioned previously. However, the majority of the current works were done by experiments, only very limited number of researches were through molecular dynamics simulation, even fewer dealt with bicrystal involving grain boundaries.

So far, several kinds of twin boundaries and tilt boundaries in $SrTiO_3$ have been observed and determined. And furthermore, investigations on atomic structure, electronic structure, and defect energetics in selected $SrTiO_3$ symmetric tilt grain boundaries were being made by a first-principles projector augmented wave (PAW) calculation,[19,20] which revealed the relationships among the atomic structure, GB energy, and GB defect energetic. In this chapter, three types of tilt grain boundaries: [001](310) $\Sigma 5$, [001](210) $\Sigma 5$ and [001](510) $\Sigma 13$ will be employed; The $\Sigma 13$ type GB contains two different cases, with different rigid-body translations of one grain with respect to the

other. The two cases stand for GBs with two energy states: stable and metastable, respectively. So, totally four different $SrTiO_3$ tilt grain boundaries will be modeled, and their Kapitza conductance will be measured.

Kapitza Resistance and Conductance

Interfacial thermal resistance, also known as thermal boundary resistance or Kapitza resistance, is a measure of an interface's resistance to thermal flow. It has been recognized that between two dissimilar materials there exists a temperature discontinuity at the interface if heat flux is applied across it,[21,22] namely, there is an interfacial thermal resistance.

The Kapitza resistance R_k is defined as follow:

$$R_k = \frac{\Delta T}{J}, \tag{4-1}$$

where ΔT is the temperature discontinuity at the interface (for here, the grain boundary), and J is the thermal current. The Kapitza conductance, σ_k , is simply the reciprocal of the Kapitza resistance R_k , and is thus defined as:

$$\sigma_k = \frac{1}{R_k} = \frac{J}{\Delta T}. \tag{4-2}$$

The relationships among the Kapitza conductance, resistance and thermal conductivity are as follows:

$$\sigma_k = \frac{\kappa}{L}, \tag{4-3}$$

$$R_k = \frac{L}{\kappa}, \tag{4-4}$$

where L is the thickness or length of the specimen along which direction heat current is applied.

In phonon-mediated thermal transport, the scattering of phonons at interfaces will lead to the rise of Kapitza resistance.[23] There are usually two theoretical frameworks that can be employed to study this interfacial resistance: the acoustic mismatch model (AMM) and the diffuse mismatch model (DMM).[23,24] The AMM says if the acoustic impedances of a material on two sides are different, there will be phonon scattering occurring at the interface. The acoustic impedance is defined as:[25,26]

$$Z = \rho c , \tag{4-5}$$

where ρ is the density and c is the speed of sound. For that the AMM is derived within continuum acoustics, it thereby has a limitation; It ignores the structure of the interfaces, which contain important information on how phonon scattering actually takes place. The DMM, by contrast, takes into account the effect of interface scattering. It is assumed that incident phonon waves will be scattered when they go through the interfaces. However, both two models cannot always provide results be in good agreement with those from the experiments.[27]

Fortunately, we have several different simulation-based approaches that can be used to study the thermal conductance of a material. Among them, the most remarkable one should be phonon wave-packet dynamics,[28] which was developed to provide a way to gain detailed insight into the mechanism of phonon scattering at interfaces. However, it doesn't seem to be easy when dealing with complex systems, such like the cases considered here. The Green-Kubo method, a representation of equilibrium MD approach, can be employed to measure the thermal conductivity of a homogeneous

system, as mentioned previously. Nevertheless, it is not appropriate to apply it into an inhomogeneous system especially when there involves localized features such as GBs studied here, for the Green-Kubo formalism was designed to handle situations being homogeneous only. Another approach, the nonequilibrium MD simulation method, which has already been successfully employed to calculate the thermal conductivity in the bulk crystal systems, will also be introduced here. Since it's a method analogous to experiments, it is much more generous. As a result, it is capable of dealing with both homogeneous and inhomogeneous situations. Although the direct method has some limitation in the ability of extracting detailed information regarding the phonon waves contacting with boundaries, it has another big advantage: being able to determine the Kapitza conductance σ_k within a single simulation.

Coincident Site Lattice Theory

The coincident site lattice (CSL) provides a relatively easy way to study and understand the structure of grain boundaries with special orientations between them. A coincident site lattice can be defined when a finite fraction of lattice sites on two lattices coincide with each other. Usually, we use the notation Σ followed by a number to express the CSL type grain boundaries. The sigma value is defined as the ratio between the area enclosed by a unit cell of the coincidence sites and that enclosed by standard ones. For example, Figure 4-1 shows a 53° ($\Sigma 5$) tilt grain boundary in cubic crystal lattice. If the area of the smaller square in dotted line (enclosed by efgh) is defined as 1, the area of the larger one (enclosed by abcd) should be 5. Thus, the ratio between the two areas is 5, which leads to the sigma value to be 5, according to the definition.

It's clear that for every specific rotation angle, if exists, one and only one sigma value can be found. However, the rule doesn't apply when a sigma value is given. In other words, the number of the possible angles corresponding to a sigma value is not limited to only one. As in the example shown in Figure 4-2, we may easily find that for a sigma value of 5, not only a rotation angle of 53°, but also 36.9° exists. The tilt grain boundary shown in Figure 4-2 is very similar to that in Figure 4-1. The only difference is the relative rotation angles between two grains. We should notice that, though the area enclosed by abcd is 10 times that enclosed by efgh, it doesn't mean we can draw the conclusion that the sigma value is 10. However, we should count in the coincidence lattice sites located in the center of each cell, and connect them with the nearest sites as presented in Figure 4-2 (the dotted square agdi). Then, the true sigma value can be obtained by calculating the ratio of area agdi, which represents the smallest CSL cell to area efgh.

From the above, we can see that for cubic cases, whenever an even sigma value appears, there should always be another coincidence site located in the center of the cell which will lead the true value to be half of the apparent quantity.

Modeling of $SrTiO_3$ Bicrystal Systems with Tilt Grain Boundaries

As the same technique, namely the direct method, will be employed to study the thermal conductance of $SrTiO_3$ tilt grain boundaries here, the procedure should be similar in spirit to that of the measurement of thermal conductivity of $SrTiO_3$ bulk crystal. However, there are still some issues we need to address first.

The first, and the most significant one is how we design a simulation model that keeps both accuracy and efficiency. For the bulk crystal system, due to the fact that

along any direction it's isotropic, simply repeating the unit cell in a specific dimension may satisfy any size demanded. But in the bicrystal case, there exists an additional inhomogeneous region, the grain boundary, which needs further transformation and adjustment in order to match well with both two crystals. Furthermore, it involves rigid body translation of one crystal with respect to the other, which makes it even harder to apply the periodic boundaries to the simulation box.

Firstly, we need to determine the approximate size of the system. Based on the previous experience, a system of $3\times3\times37$ unit cells should be ok in order to get comparable results. Then, a single crystal block about twice as large as the approximate size is generated. It's necessary to obtain a relatively big blank at first since it makes sure when further manipulations are done, the part we want is still available. After that, we rotate the model chunk by an angle around the designated axis, according to the grain boundary type. For here, our goal is to create a bicrystal model with [001](310)$\sum$5 grain boundaries, which means the rotation axis may be any of the three coordinate axes. We simply use the y axis as shown in Figure 4-3. And the rotation angle should be 18.435 degree. The next step is to cut out the middle portion, which is a single crystal, of the simulation system. In order to make sure the structure is stable and keeps charge neutrality, we have to find out two characteristic atoms located on the two grain boundary planes on each side of the central crystal, respectively, and set up two borders. In this case, the characteristic atom type is chosen to be Titanium, since it will appear on the boundary planes. Then, all atoms stay within the two borders will be kept and everything else outside will be cut off. The resulting geometry is shown in Figure 4-4A. Next, we divide the remaining central part into two sections, the left and

the right. The left section is further made a mirror copy with respect to the left border plane and right section also makes a mirror copy with respect to the right border. The resulting geometry is shown in Figure 4-4B. Although the model looks like it has three pieces, actually it contains only two single crystals. Since periodic conditions will be applied to both left and right boundaries, the two parts adjacent to the two boundaries will be connected and matched as a single crystal. Before cutting out the final model, we still have another important step need to do first. According to the study on GB energy of $SrTiO_3$ by Imaeda et al,[19] a rigid body translation of one grain with respect to the other is necessary in order to minimize the grain boundary energy and stabilize the structure. Thus, the grain in the middle stays and the remaining parts are subject to a rigid body translation to the proper positions, as shown in Figure 4-5. For the case here, the corresponding translation vector is (-4.5, 0.5, 0.5) (in Angstrom). Figure 4-6 shows the final model, which is obtained by cutting off the excess part of the roughcast.

Molecular Dynamics Simulation of Kapitza Conductance at Grain Boundaries

The results the from the previous chapter on measurement of thermal conductivity of bulk crystal show that the nonequilibrium MD simulation method is suitable to be employed to evaluate the thermal properties in this ionic-bonded perovskite type material. Thus, the same technique is used to simulate the bicrystal systems with tilt grain boundaries.

We make use of the modeling procedure developed in the last section and generate totally four models of different GB configurations: [001](310)Σ 5, [001](210)Σ 5, [001](510)Σ 13 stable and [001](510)Σ 13 metastable, as shown in Figure 4-7. Due to the excessive length along z directions, only a half of the model is presented for each

case. The figures on the left are models viewed along y direction and those on the right are models viewed along x direction.

The schematic representation of the three-dimensional simulation cell is shown in Figure 4-8. Each model is bounded in a simulation box has the exact matching size, with periodic border conditions in all three directions applied. That means the boundaries along x and y directions are infinitely extended and the heat current will go along z direction only, which is very similar to the technique used in finite element analysis. And because of the periodicity in the z direction, the system can thus be regarded as a simulation cell containing two crystals joined by two crystallographically identical but symmetric tilt grain boundaries. The heat current along the negative z direction will leave the left border and go back from the right border again forming a loop. At each MD time step (0.55fs), we rescale the particle velocities at two thin slabs, one located in the middle of the simulation cell and the other near the right border. Each of the two slabs keeps a same distance from both of the two grain boundaries in order to get a symmetric temperature profile. The thickness of the slabs doesn't matter much as is already discussed, we thus simply choose it to be 6 Å, according to the length of the whole system. To create a heat current, we add some energy $\Delta\varepsilon$ at each MD step to one slab and remove the same amount of energy $\Delta\varepsilon$ from the other slab, which always conserves the total energy of the whole system. The heat current can thus be calculated through the equation:

$$J = \frac{1}{2A}\frac{\Delta\varepsilon}{\Delta t}, \tag{4-6}$$

where A is the transversal area of the cross section (lies in xy plane), Δt is the MD time step, 1/2 means the amount of energy $\Delta\varepsilon$ added into the heat source is split into two

equal parts, going through two ways as indicated in Figure 4-8, we only need to consider one way when doing calculation. Since we have known the heat current flowing in the system, the thing we care about left is the temperature discontinuity at the two grain boundaries, which may be measured from the temperature profile when the whole system achieves a steady state.

The whole simulation procedure consists of four steps: initiating velocity, environmental temperature control, microcanonical relaxation and applying heat flux, which is basically the same as that in thermal conductivity measurement. It has already been known in the previous chapter that 200,000 to 300,000 steps after constant heat flux is applied should be long enough for the whole system to achieve the dynamic steady state. We thus extract out the temperature data at each point along z direction, with an interval of 4 angstroms, for the time steps from 500,000 to 2,000,000, and do the average. Then a smooth temperature profile will be seen and the post processing can be done.

Results and Discussion

The final temperature profiles of the four bicrystal systems are shown in Figure 4-9. Comparing with the results getting from the silicon bicrystal systems, we may easily find that the temperature discontinuities are very sharp here although drops are not that steep like those happening at silicon grain boundaries. The large temperature variation in the GB region indicates there exists a high thermal resistance, or equivalently, a low thermal conductance. However, It is not easy to quantitatively evaluate the Kapitza conductance here since the temperature doesn’t come in with a sudden jump but with a transitional curve with finite gradient. This is because of the high computational cost of ionic-bonded materials, our models cannot be created in large sizes, like those in silicon.

Thus, it's necessary to develop a method to quantitatively determine the temperature discontinuities in our cases. Figure 4-10 shows how the issue is addressed. We break the data into two parts, the left part and the right part, and inspect the left first. We need to perform a function fitting for the raw data first, since they come in with discrete form. In order to keep as much information as possible from the original data, we choose the polynomial model of rank 12, which has the ability to mimic complex curves. We then take the derivative of the fitted function twice and find out the stationary points for the temperature gradient curve, which can obtained by taking the derivative of the temperature distribution curve once, as shown in Figure 4-10B, blue dashed curve. The positions of the stationary points are where temperature gradient alters its trend of changing, which in other words are potential boundaries of the area whose Kapitza conductance is affected by the presence of the GB. Because of the fluctuations of the temperature distribution curve due to the existence of inherent errors, we may find several stationary points in each curve, as we can see from Figure 4-10 and Figure 4-11. However, only two of them are "real", or meaningful. Fortunately, they can be easily distinguished from the figure. As an example, in Figure 4-10B, the two meaningful points are the two adjacent to the centered point which corresponds to the extreme value in the 1st derivative curve. After the two points are located, their positions along z direction are known, and the corresponding two temperature values can be obtained from the temperature distribution curve. The difference of these two values, i.e. ΔT , will be used to evaluate the Kapitza conductance.

Table 4-1 summarizes the measured temperature discontinuities at each grain boundary, with same heat current applied (1.791e11 W/m^2) in each case. Since in every

step same amount of energy is added to the heat source and equivalent amount of energy is subtracted from the heat sink, and NVE control maintains at the same time, the total energy is always conserved, which makes the mean temperature of the whole system stay at 600K. After the temperature discontinuities at both GBs in each system are measured, we take the average and apply Equation 4-2, to get the Kapitza conductance. The calculated results are also included in Table 4-1. As we can see, the (510)Σ13 metastable GB has the largest σ_k value while (310)Σ5 possesses the lowest thermal conductance. Interestingly, the same GB type with same misorientation angle but with different rigid-body translation could show very diverse results. If we look at the σ_k values of Σ13 grain boundaries, we may find that Kapitza conductance of the stable boundary is about 25% lower than that of the metastable boundary, which is unexpected since the disparity is even greater than those between different GB types. However, we have to admit there may exist some relationship between the thermal conductance and the grain boundary energy, since the GB energy values of the two configurations are not close as well. Table 4-2 lists the GB energy for each type of the grain boundary and their rigid-body translation vectors. The data are from the study by M. Imaeda and co-workers[19] and the study by H. –S. Lee and co-workers.[20] From the table, we may find the Σ13 stable structure has the lowest GB energy among the four while the Σ13 metastable structure has the largest. However, the trend of the correlation between the GB energy and σ_k value we got here is opposite to that reported by Schelling and co-workers[23] for Silicon boundaries. While Schelling found the high-energy, disordered grain boundary has a smaller value of σ_k if compared to the

lower-energy, more ordered grain boundary, we observed that the metastable grain boundary with a higher energy shows a stronger ability to pass the heat current, i.e., a higher Kapitza conductance, while the stable grain boundary with much lower GB energy shows a rather smaller σ_k value, for the $\Sigma 13$ grain boundaries.

Then we try to gain more information from the geometric constructions of the grain boundaries. Figure 4-12 are the snap shots of the grain boundary structures of the four systems after they are dynamically stabilized. We can find that except for the (210) $\Sigma 5$ case, all other three models show big voids at the boundary. Especially for (310) Σ 5 boundary, the boundary line is almost made up with continuous cavities, with only few number of atoms connecting the two grains, which makes it not difficult to understand why this type of grain boundary possesses a low σ_k value (lowest among the four).By contrast, the $\Sigma 13$ stable structure shown in Figure 4-12C has a higher thermal conductance value than the (310) $\Sigma 5$ case although it also has comparable sized voids at the boundary. This is because there is a higher density of atoms joining the two grains here, which makes the bridge to connect the two regions wider. As a result, more phonons will be able to pass through. Comparing A, B and C three cases in Figure 4-12 and their corresponding σ_k values, we may easily find that voids at boundaries may impede the thermal transport, but what's more, the amount of atoms connecting the left and right part plays a more important role. However, we cannot make a judgement by only looking at the clues found above. There are other factors that may be also critical. We should have noticed that the $\Sigma 13$ metastable grain boundary (Figure 4-12D)is kind of special. Though its structure is very alike to that $\Sigma 13$ stable structure as shown in

Figure 4-12C, it has a much higher Kapitza conductance, ever higher than the (210) $\Sigma 5$ boundary, which shows no obvious big voids. But if we inspect the atom alignments in the GB region, we may find the pattern in metastable structure is much more ordered if compared with that in stable structure, where disorders such as dislocations are observed. This suggests that the amount of disorder at grain boundary can have significant effect.

Furthermore, it is noticed that temperature discontinuities measured at the two GBs are slightly different in each case, as we can see in Table 4-1, though same conditions and periodic borders are applied. There must be some other reasons since the variation is already beyond the range of statistical errors. We make a comparison between the left GB structure and the right GB structure, as shown in Figure 4-13. To make life easier, we simply rotate the left GB by 180 degrees to make it comparable to the right boundary. We see the two incident planes are different, or more precisely, they are symmetric. This is a potential factor that may change the behavior of phonon propagation. However, it's beyond my scope, investigations on phonon wave dynamics will be needed in order to elucidate this.

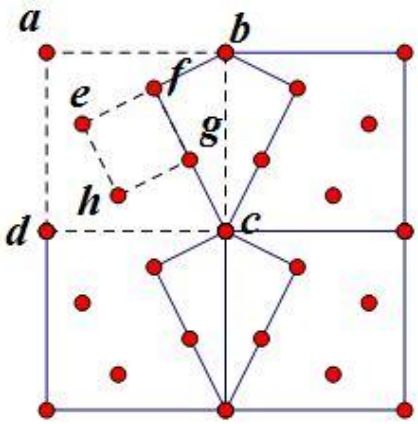

Figure 4-1. Schematic representation of a 53° ($\Sigma 5$) tilt grain boundary in cubic crystal lattice. The ratio of the area enclosed by abcd to that enclosed by efgh is 5.

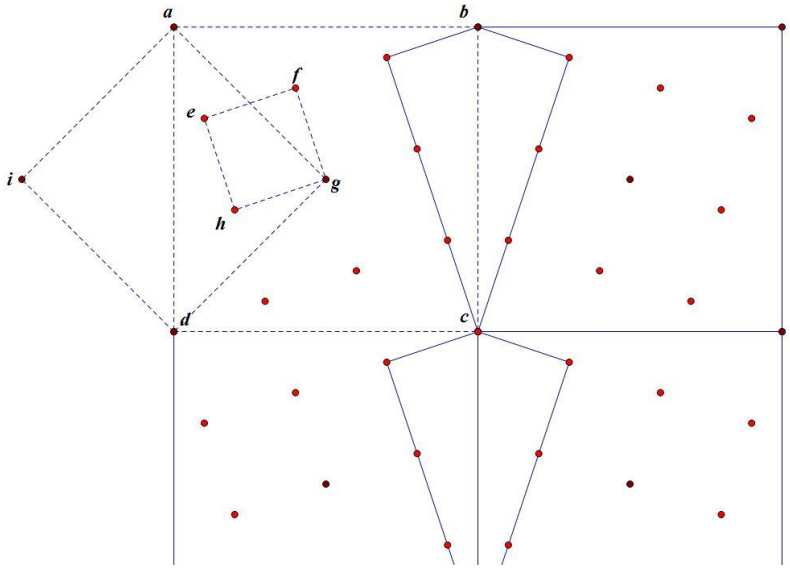

Figure 4-2. Schematic representation of a 36.9° ($\Sigma 5$) tilt grain boundary in cubic crystal lattice. The ratio of the area enclosed by agdi to that enclosed by efgh is 5.

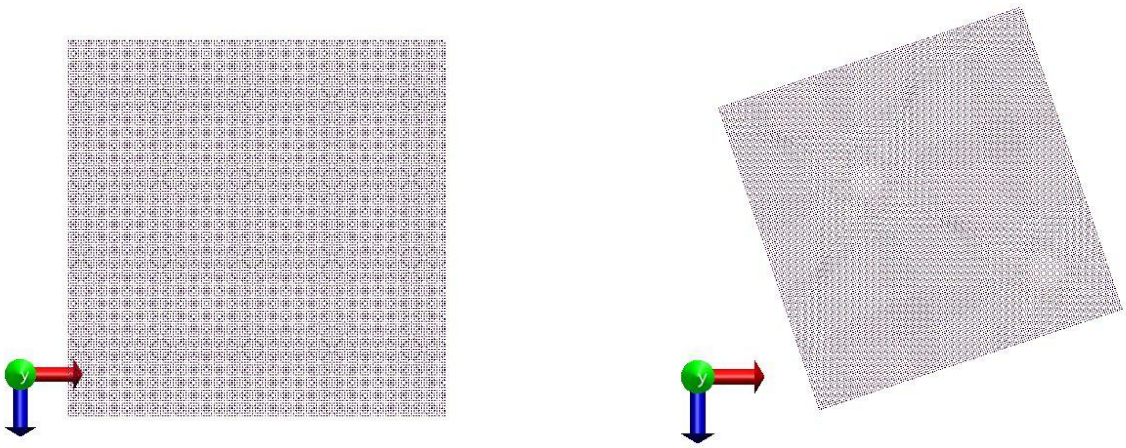

A B

Figure 4-3. $SrTiO_3$ bicrystal modeling procedure. A) Generating a single crystal with size about twice as large as the approximate final one. B) Rotating the model by an angle according to the grain boundary type. In this case, [001](310)∑5 grain boundary, the angle should be 18.435° .

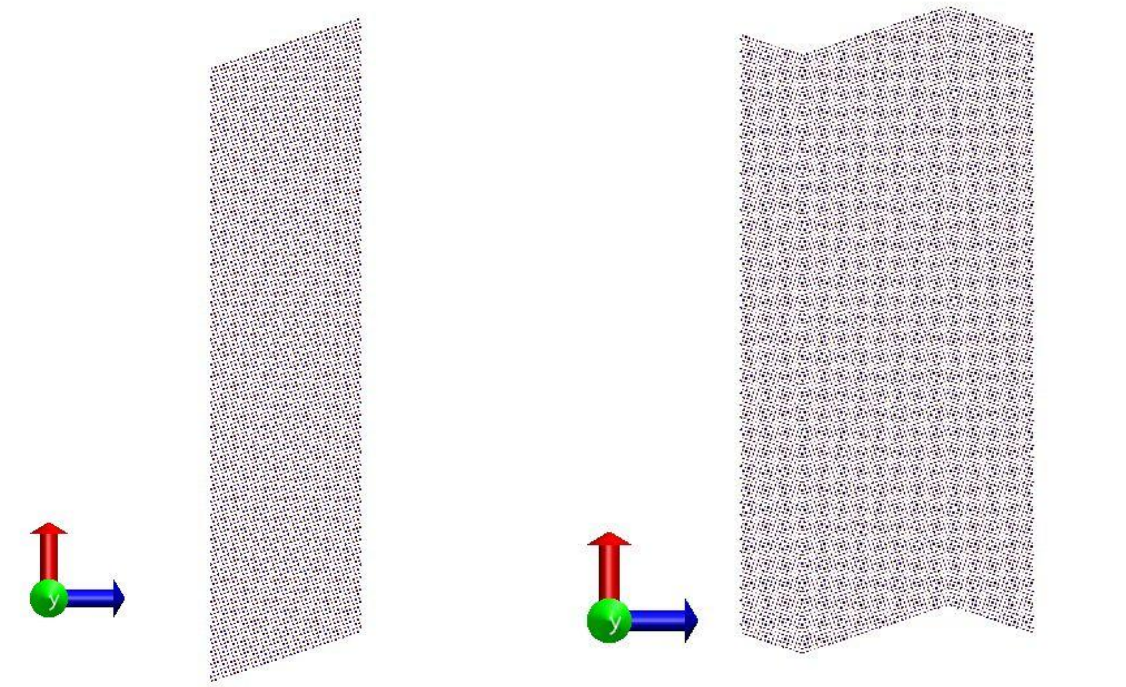

A B

Figure 4-4. $SrTiO_3$ bicrystal modeling procedure, continued. A) Cutting out the middle part (the first single crystal) of the bicrystal system. B) Generating the second single crystal based on the first part by mirror copy.

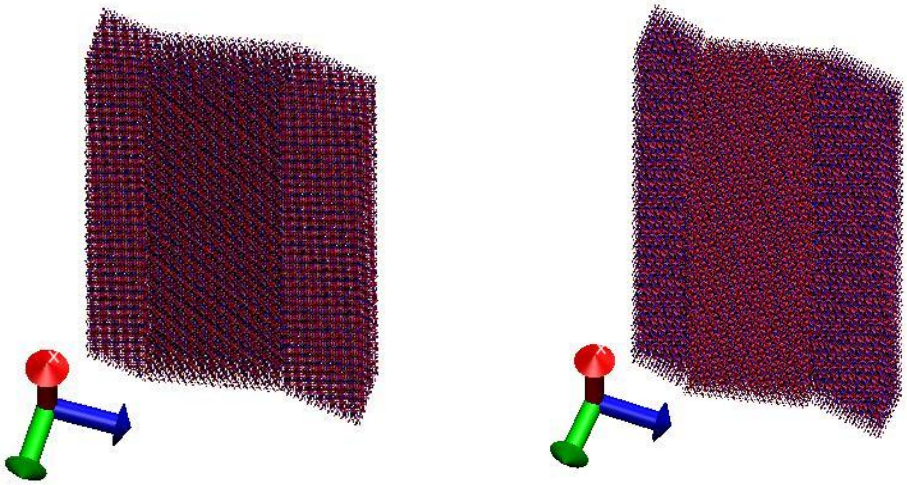

A B

Figure 4-5. $SrTiO_3$ bicrystal modeling procedure, continued. A) before rigid body translation, B) after rigid body translation.

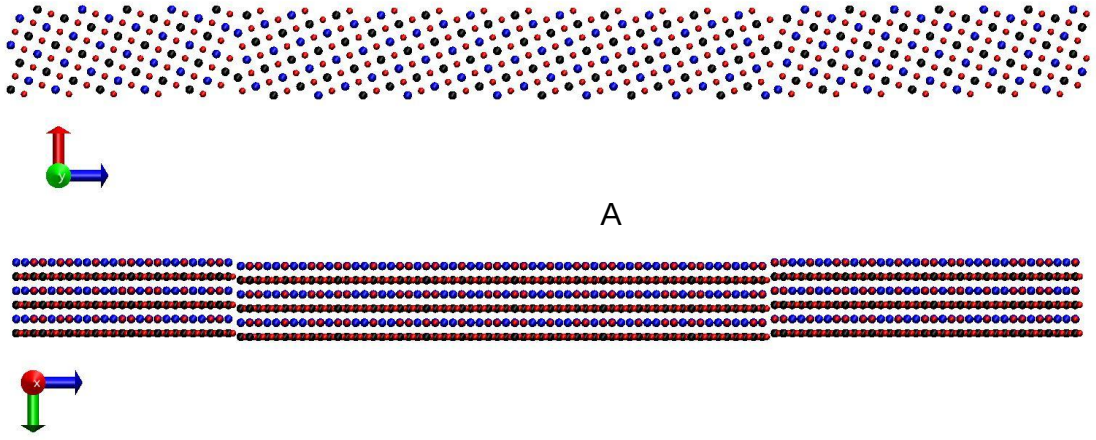

A

B

Figure 4-6. Cutting out the final model. A) view along y direction, B) view along x direction.

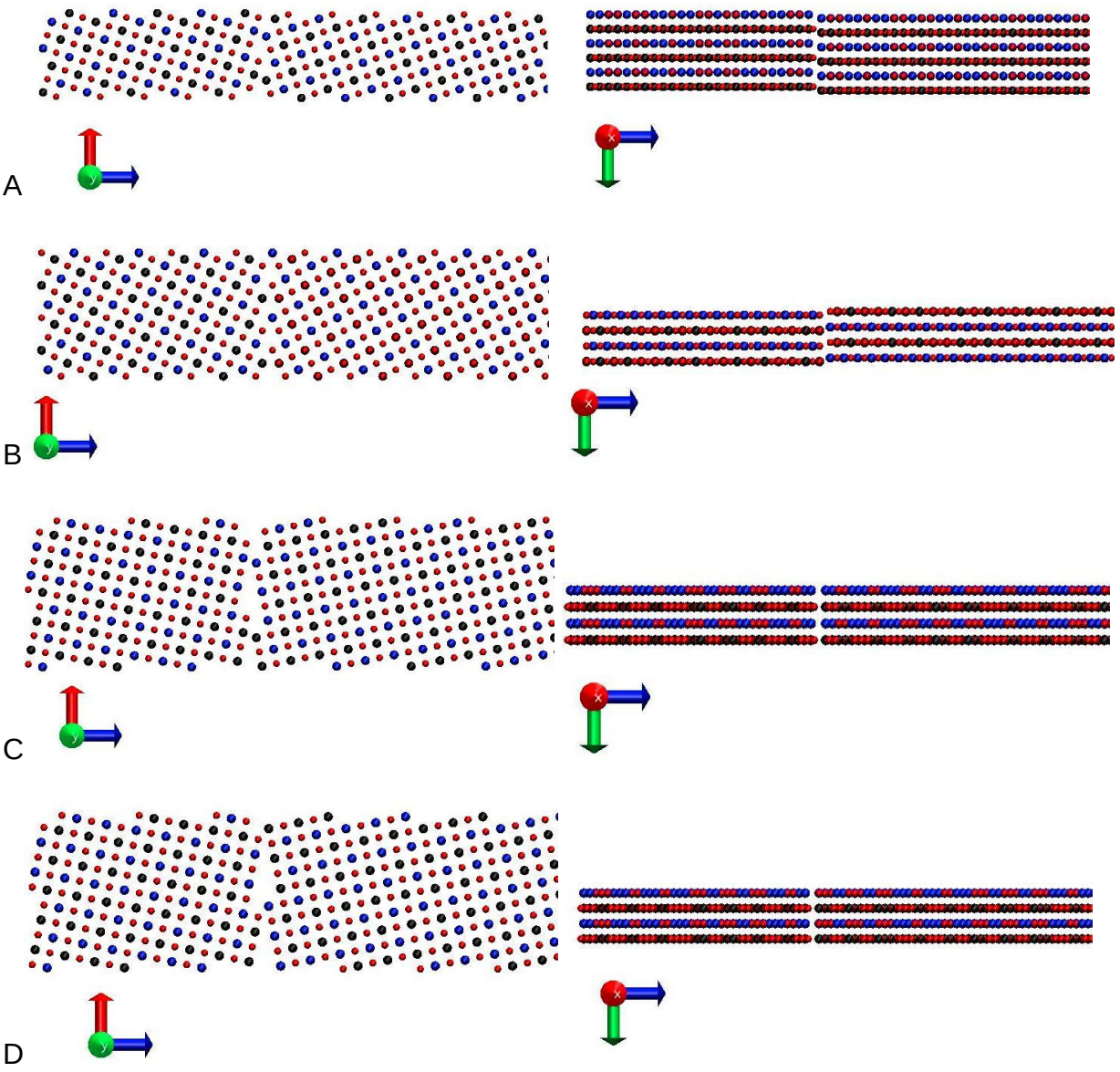

Figure 4-7. Four $SrTiO_3$ bicrystal models (partial view, only left side of the model is shown) with different GB configurations. A) [001](310)Σ5, B) [001](210)Σ5, C) [001](510)Σ13 stable state, D) [001](510)Σ13 metastable state.

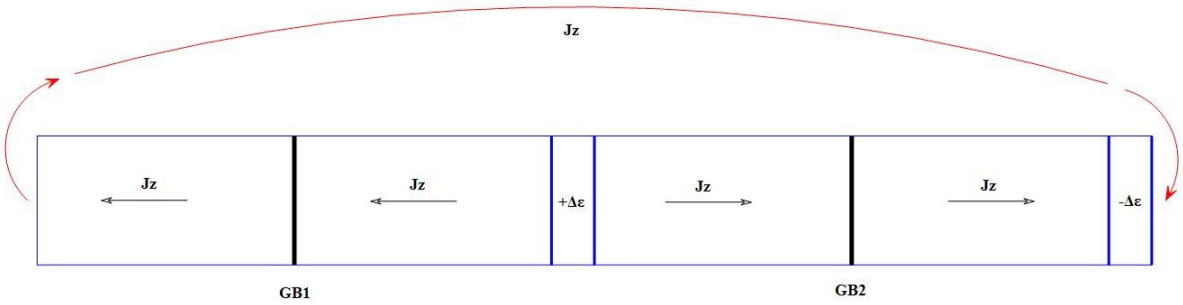

Figure 4-8. Schematic representation of the three-dimensional periodic simulation cell.

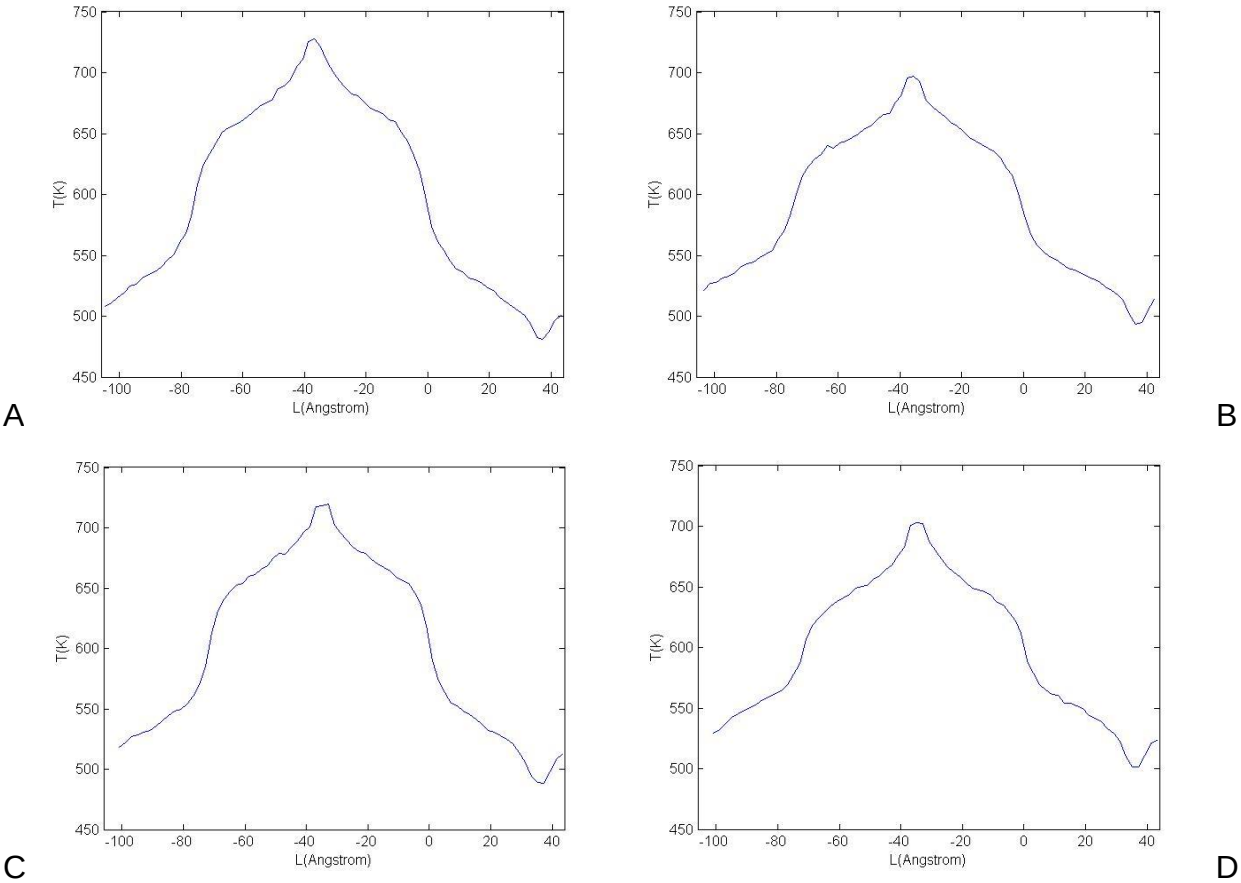

Figure 4-9. Temperature profiles of four bicrystal systems with a steady thermal current of 1.7910e+011 W/m^2 applied along the z direction, averaged over 500,000 to 2,000,000 time steps. The background temperature is controlled at 600 K. A) [001](310)Σ5, B) [001](210)Σ5, C) [001](510)Σ13 stable state, D) [001](510)Σ13 metastable state.

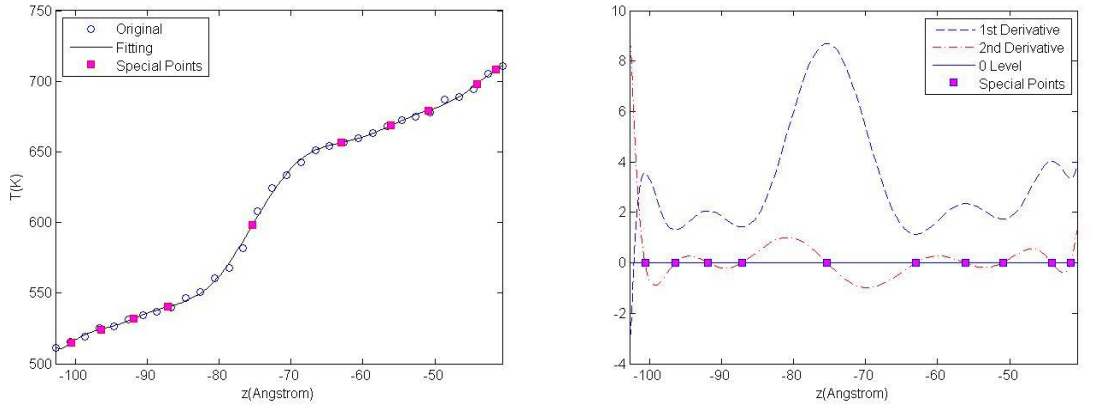

A B

Figure 4-10. Data analysis of the left part of the temperature profile. A) Fit the temperature profile using order 12 polynomial, B) Find positions where trends shift, using the 2nd order derivative.

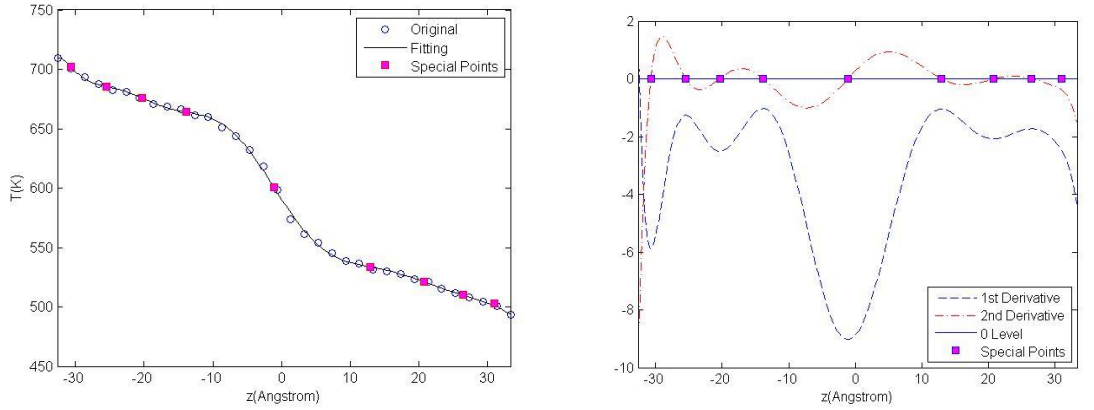

A B

Figure 4-11. Data analysis of the right part of the temperature profile. A) Fit the temperature profile using order 12 polynomial, B) Find positions where trends shift, using the 2nd order derivative.

Table 4-1. Measured temperature discontinuities and the corresponding Kapitza conductance for the four tilt grain boundaries at T=600K. The heat current applied is 1.7910e+011 W/m^2.

GB type	$\Delta T(K)$ at left boundary	$\Delta T(K)$ at right boundary	$\Delta T(K)$ averaged	$\sigma_k(GW/m^2K)$
[001](310)Σ5	116.20	130.60	123.40	1.45
[001](210)Σ5	91.70	99.00	95.35	1.88
[001](510)Σ13 stable	107.50	116.20	111.85	1.60
[001](510)Σ13 metastable	78.40	89.00	83.70	2.14

Table 4-2. Rigid body translations of one grain with respect to the other for the four systems and the corresponding GB energy. ※Data from M. Imaeda and co-workers and H. –S. Lee and co-workers.[19,20]

GB type	Rigid body translation x(Å)	Rigid body translation y(Å)	Rigid body translation z(Å)	GB energy (J/m^2)
[001](310)Σ5	-4.5	0.5	0.5	1.02
[001](210)Σ5	0.0	1.5	0.5	0.98
[001](510)Σ13 stable	-4.5	0.0	1.0	0.93
[001](510)Σ13 metastable	-10.5	0.0	1.0	1.37

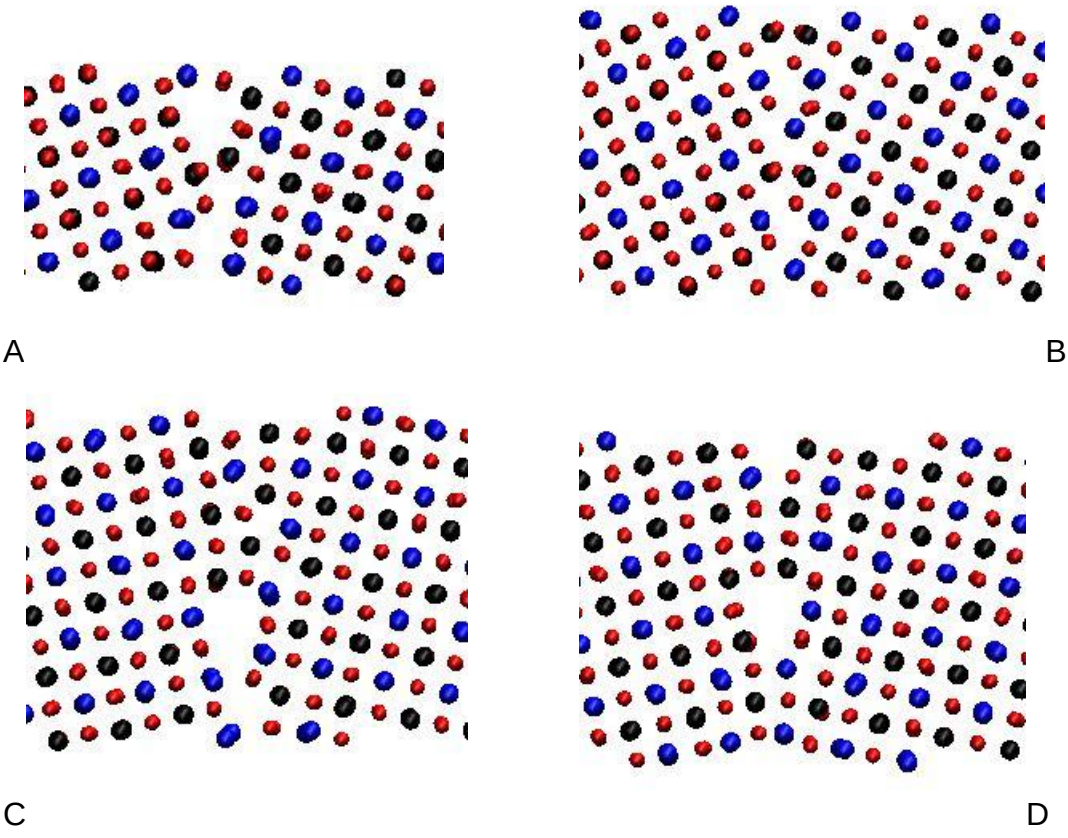

Figure 4-12. Snap shot of the right grain boundary region, after the system is dynamically stable. A) [001](310)Σ5, B) [001](210)Σ5, C) [001](510)Σ13 stable, D) [001](510)Σ13 metastable.

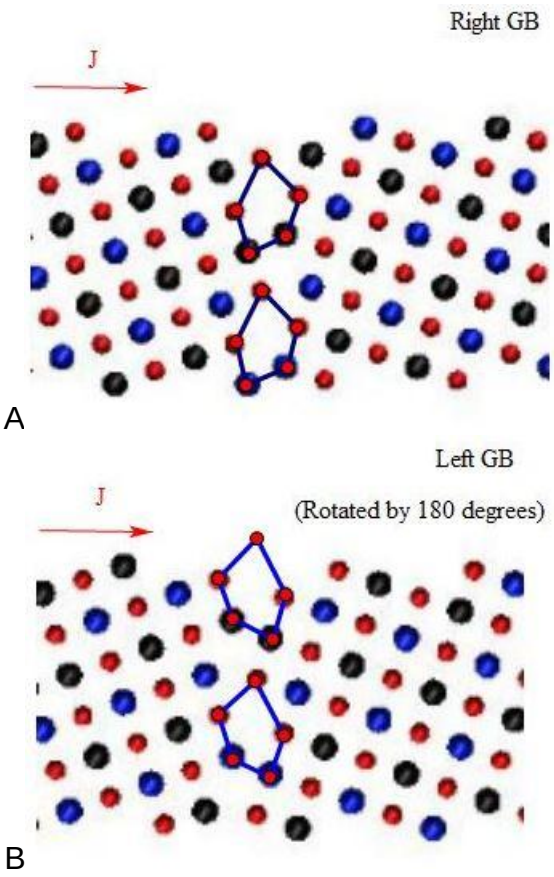

Figure 4-13. Comparison of left and right grain boundary structure at the original 310 GB model. A) GB structure on the right, the positive z direction points to the right; B) GB structure on the left, the positive z direction points to the left (rotated by 180 degrees). The direction in which heat flows is indicated in red arrows.

CHAPTER 5
CONCLUSIONS

We measured the thermal conductivity of $SrTiO_3$ bulk crystal using the nonequilibrium molecular dynamics simulation first and systematically explored the related issues coming with the method. It is found that a heat current density value of $1.791\times10^{11}\ W/m^2$ should be suitable for the simulation since the stimulation is strong enough for the system to quickly achieve a smooth temperature profile and the resulting thermal conductivity values show almost no deviation from Fourier's law. The study on the dependence of κ values on cross-sectional area shows the system with a cross section size at least 3 by 3 unit cells will be required to obtain a reliable result.

The final values are extrapolated and compared with those from experiments and other simulations, which shows a reasonable agreement, indicating that the method works well with the material studied here. Then, four bicrystal systems with different symmetric tilt grain boundaries (Σ5(310), Σ5(210), Σ13(510) stable, and Σ13(510) metastable) are modeled and their Kapitza conductance at grain boundaries are evaluated by simulations using the same, well tested technique. We compare the results and find the Kapitza conductance depends on the amount of disorder at grain boundary region most, but doesn't show direct relationship with the GB energy. This can be seen from the two Σ13 structures. The stable structure possessing the lowest GB energy among the four shows an intermediate thermal conductance while the metastable one with the highest GB energy but an ordered structure shows the strongest ability to pass the heat flux through. We also find the voids and gaps may impede the thermal transport and their density along the grain boundary plays an important role. Finally, we notice that temperature discontinuities measured at the two

grain boundaries are slightly different in each case. The two GBs have exactly the same structure but face towards opposite directions, which means from which side the incident heat current comes also matters. This suggests the pattern of an incident plane may be a factor to influence the thermal transport. However, further investigations on larger systems and studies about phonon wave dynamics will be necessary in order to elucidate this.

LIST OF REFERENCES

[1]T. Okuda, K. Nakanishi, S. Miyasaka, and Y. Tokura, Phys. Rev. B 63, 113104 (2001).

[2]G. G. Yadav, G. Zhang, B. Qiu, J. A. Susoreny, X. Ruan, and Y. Wu, Nanoscale 3, 4078 (2011).

[3]Y. Wang, K. Fujinami, R. Zhang, C. Wan, N. Wang, Y. Ba, and K. Koumoto, APEX 3, 031101 (2010).

[4]H. Iwahara, T. Yajima, T. Hibino, and H. Ushida, J. Electrochem. Soc. 140, 1687 (1993).

[5]N. Kurita, N. Fukatsu, and T. Ohashi, J. Spn. Inst. Metals 58, 782 (1994).

[6]T. Yajima, K. Koide, H. Takai, N. Fukatsu, and H. Iwahara, Solid State Ionics 79 333 (1995).

[7]G. S. Nolas, D. T. Morelli, and T. M. Tritt, Annu. Rev. Mater. Sci. 29, 89 (1999).

[8]A. Chernatynskiy, R. W. Grimes, M. A. Zurbuchen, D. R. Clarke, and S. R. Phillpot, Appl. Phys. Lett. 95, 161906 (2009).

[9]H. Muta, K. Kurosaki, and S. Yamanaka, J. Alloys Compd. 392, 306 (2005).

[10]B. S. Thomas, N. A. Marks, and B. D. Begg, Nucl. Instrum. Methods Phys. Res., Sect. B 228, 288 (2005).

[11]A. Chernatynskiy, J. E. Turney, A. J. H. McGaughey, C. H. Amon, and S. R. Phillpot, J. Am. Ceram. Soc. 94, 3523 (2011).

[12]S. Yamanaka, K. Kurosaki, T. Maekawa, T. Matsuda, S. Kobayashi, and M. Uno, J. Nucl. Mater.344, 0161 (2005).

[13]T. Seetawan, G. Wong-ud-dee, C. Thanachayanont, and V. Amornkitbumrung, Chinese Phys. Lett. 27 (2) 026501 (2010).

[14]T. Yamamoto, Y. Sato, T. Tanaka, K. Hayashi, Y. Ikuhara, and T. Sakuma, J. Mater. Sci. 40, 881 (2005).

[15]M. Fujimot and W. D. Kingery, J. Am. Ceram. Soc. 68, 169 (1985).

[16]D. Dimos, P. Chaudhari, and J. Mannhart, Phys. Rev. B 41, 4038 (1990).

[17]C. C. Tsuei, J. R. Kirtley, C. C. Chi, L. S. Yujahnes, A. Gupta, T. Shaw, J. Z. Sun, and M. B. Ketchen, Phys. Rev. Lett. 73, 593 (1994).

[18]P. Chaudhari, J. Mannhart, D. Dimos, C. C. Touri, J. Chi, M. M. Oprysko, and M. Scheuermann. ibid. 60, 1653 (1988).

[19]M. Imaeda, T. Mizoguchi, Y. Sato, H. –S. Lee, S. D. Findlay, N. Shibata, T. Yamamoto, and Y. Ikuhara, Phys. Rev. B 78, 245320 (2008).

[20]H. –S. Lee, T. Mizoguchi, J. Mistui, T. Yamamoto, S. –J. L. Kang, and Y. Ikuhara, Phys. Rev. B 83, 104110 (2011).

[21]P. L. Kapitza, J. Phys. USSR 4, 181 (1941).

[22]E. T. Swartz and R. O. Pohl, Rev. Mod. Phys. 61, 605 (1989).

[23]P. K. Schelling, S. R. Phillpot, and P. Keblinski, J. Appl. Phys. 95, 6082 (2004).

[24]S. Aubry, C. J. Kimmer, A. Skye, and P. K. Schelling, Phys. Rev. B 78, 064112 (2008).

[25]E. T. Swartz and R. O. Pohl, Rev. Mod. Phys. 61, 605 (1989).

[26]I. M. Khalatnikov, Zh. Eksp. Teor. Fiz. 22, 687 (1952).

[27]R. M. Costescu, M. A. Wall, and D. G. Cahill, Phys. Rev. B 67, 054302 (2003).

[28]P. K. Schelling, S. R. Phillpot, and P. Keblinski, Appl. Phys. Lett. 80, 2484 (2002).

BIOGRAPHICAL SKETCH

Zexi Zheng was born in Shanghai, China, in 1989. After he finished his high school studies at No.2 Secondary School Attached to East China Normal University, he took the college entrance examination and was admitted to the School of Mechanical and Vehicular Engineering at Beijing Institute of Technology (BIT), Beijing, China, in 2007. He earned his Bachelor of Engineering degree from BIT with a major in automotive engineering in 2011. Then he got his admission to the Department of Mechanical and Aerospace Engineering at the University of Florida and came to Gainesville, Florida in August, 2011. He worked with Dr. Youping Chen in the Atomistic and Multiscale Mechanics Group since 2011. He received his M.S. in mechanical engineering from the University of Florida in the spring of 2013.